The Astrophysical Journal, 629:686–699, 2005 August 20

XMM-NEWTON VIEW OF PKS 2155−304: CHARACTERIZING THE X-RAY VARIABILITY PROPERTIES WITH EPIC pn

Y. H. Zhang
Department of Physics and Tsinghua Center for Astrophysics, Tsinghua University, Beijing 100084, China;
youhong.zhang@mail.tsinghua.edu.cn

A. Treves
Dipartimento di Scienze, Università degli Studi dell'Insubria, via Valleggio 11, I-22100 Como, Italy

A. Celotti
International School for Advanced Studies, SISSA/ISAS, via Beirut 2-4, I-34014 Trieste, Italy

and

Y. P. Qin and J. M. Bai
National Astronomical Observatories/Yunnan Observatory, Chinese Academy of Sciences,
P.O. Box 110, Kunming, Yunnan 650011, China
Received 2005 January 25; accepted 2005 May 3

ABSTRACT

Starting from *XMM-Newton* EPIC pn data, we present the X-ray variability characteristics of PKS 2155−304 using a simple analysis of the excess variance, $\sigma_{\rm XS}^2$, and of the fractional rms variability amplitude, $F_{\rm var}$. The scatter in $\sigma_{\rm XS}^2$ and $F_{\rm var}$, calculated using 500 s long segments of the light curves, is smaller than the scatter expected for red-noise variability. This alone does not imply that the underlying process responsible for the variability of the source is stationary, since the real changes of the individual variance estimates are possibly smaller than the large scatters expected for a red-noise process. In fact, the averaged $\sigma_{\rm XS}^2$ and $F_{\rm var}$, which reduce the fluctuations of the individual variances, also change with time, indicating nonstationary variability. Moreover, both the averaged $\sigma_{\rm XS}$ (absolute rms variability amplitude) and the averaged $F_{\rm var}$ show linear correlation with source flux, but in an opposite sense: $\sigma_{\rm XS}$ correlates with flux, but $F_{\rm var}$ anticorrelates with flux. These correlations suggest that the variability process of the source is strongly nonstationary, as random scatters of variances should not yield any correlation. Spectra of $F_{\rm var}$ were constructed to compare variability amplitudes in different energy bands. We found that the fractional rms variability amplitude of the source, when significant variability is observed, increases logarithmically with the photon energy, indicating significant spectral variability. The point-to-point variability amplitude may also track this trend, suggesting that the slopes of the power spectral density of the source are energy-independent. Using the normalized excess variance, the black hole mass of PKS 2155−304 was estimated to be about $1.45\times10^8\ M_\odot$. This is compared and contrasted with the estimates derived from measurements of the host galaxies.

Subject headings: BL Lacertae objects: general — BL Lacertae objects: individual (PKS 2155−304) — galaxies: active — methods: data analysis — X-rays: galaxies

1. INTRODUCTION

Blazars are the extreme subclass of active galactic nuclei (AGNs): they show rapid variability on different timescales across the whole electromagnetic spectrum (Ulrich et al. 1997). A number of observational facts define our current understanding of blazars. The entire electromagnetic emission from blazars is produced by relativistic electrons tangled with the magnetic field in a relativistic jet roughly aligned with our line of sight (Blandford & Rees 1978; see Urry & Padovani [1995] for a review). TeV blazars represent a subclass whose emission has been detected at up to TeV energies with ground-based Cerenkov telescopes. The number of TeV blazars is gradually growing. Up to now, there have been six confirmed TeV blazars, including the three prototypical blazars Mrk 421, Mrk 501, and PKS 2155−304. The overall spectral energy distributions of TeV blazars show that synchrotron emission from these sources peaks at the high-energy (UV/soft X-ray) band. This indicates that the X-ray emission from TeV sources is the high-energy tail of the synchrotron emission component produced in the inner part of the relativistic jets, where the most rapid variability is expected. Therefore, TeV blazars are jet/synchrotron emission–dominated X-ray sources. They have been the important targets of various X-ray telescopes such as the *Advanced Satellite for Cosmology and Astrophysics* (*ASCA*), *BeppoSAX*, the *Rossi X-Ray Timing Explorer* (*RXTE*), *Chandra*, and *XMM-Newton*. These X-ray observations have revealed very complex variability patterns for the TeV sources (for a review, see Pian 2002).

X-ray emission from TeV blazars is known to be the most variable. The X-ray light curves obtained so far with various X-ray telescopes show aperiodic and unpredictable events (e.g., flare intensity and duration), although the flares usually occur on timescales of days as viewed from the long-look observations (e.g., Tanihata et al. 2001; Zhang et al. 2002; Cui 2004; Massaro et al. 2004). Clearly, characterizing the X-ray variability of TeV blazars is important for exploring the underlying physical processes at work. However, the X-ray variability of TeV blazars is a stochastic red-noise process, and its analysis requires a large amount of data in order to obtain meaningful *average* properties of the statistical moments of the light curves. Probably the best tool to characterize the X-ray variability is to measure the fluctuation of the power spectral density (PSD). The PSD method has been frequently used for examining the X-ray variability properties of X-ray binaries and Seyfert galaxies (e.g., Pottschmidt

TABLE 1
OBSERVATIONAL JOURNAL OF PKS 2155−304 WITH *XMM-Newton* EPIC pn

Revolution	Obs. ID	Exp. ID	Date (UTC)	Mode	Filter	Duration (10 ks)	Exposure (10 ks)	Background	Pileup
87.....	0124930101	87-1	2000 May 30 10:20:09 to May 30 20:53:29	SW	Medium	3.80	2.66	Yes	Yes
	0124930201	87-2	2000 May 31 00:52:59 to May 31 17:21:38	SW	Medium	5.93	4.16	Yes	Yes
174.....	0080940101	174-1	2000 Nov 19 19:00:40 to Nov 20 10:55:39	SW	Thin	5.73	4.02	No	Yes
	0080940301	174-2	2000 Nov 20 13:15:19 to Nov 21 05:25:19	SW	Thin	5.82	4.08	Yes	Yes
362.....	0124930301	362-1	2001 Nov 30 03:12:05 to Nov 30 15:30:29	TI	Medium	4.32	4.27	No	No
		362-2	2001 Nov 30 15:54:06 to Dec 1 04:17:30	SW	Medium	4.46	3.13	No	Yes
450.....	0124930501	450-1	2002 May 24 11:18:09 to May 24 20:08:10	SW	Medium	3.18	2.23	No	Yes
		450-2	2002 May 24 20:31:33 to May 25 05:19:52	SW	Thin	3.15	2.21	No	Yes
		450-3	2002 May 25 05:43:16 to May 25 14:01:35	SW	Thick	2.99	2.10	No	Yes
545.....	0124930601	545-1	2002 Nov 29 23:32:52 to Nov 30 15:20:17	SW	Thick	5.67	3.98	No	No
		545-2	2002 Nov 30 15:57:29 to Dec 1 07:14:54	TI	Thick	5.50	5.44	Yes	No
724.....	0158960101	724	2003 Nov 23 00:52:28 to Nov 23 08:16:59	SW	Thick	2.66	1.87	Yes	No

et al. 2003; Markowitz et al. 2003). The source's PSD represents the amount of mean variability amplitude as a function of temporal frequency (per timescale). Measuring the PSD requires rather long, high-quantity (evenly sampled), and adequate data (multiple light curves or multiple segments of a long observation) for the average PSD to have physical significance. The PSDs obtained so far for TeV blazars are only in the high-frequency range, roughly between 10^{-5} and 10^{-3} Hz. In this range the PSDs are most likely represented by a power law [$\mathcal{P}(f) \propto f^{-\alpha}$, where $\mathcal{P}(f)$ is the power at frequency f] with slope $\alpha \sim 2$–3 (Kataoka et al. 2001; Zhang et al. 1999, 2002; Zhang 2002; Brinkmann et al. 2003). However, because of periodic gaps associated with the observations gathered with low–Earth orbital satellites such as *ASCA*, *BeppoSAX*, and *RXTE*, usually one cannot perform a full PSD analysis with such data. Special treatments have to be imposed on the data before calculating a PSD.[1] Instead, a structure function (SF) that works with light curves that have gaps has been used to perform a similar analysis in the time domain. Physically, the PSD and the SF are identical only in the limit of a light-curve length with $T \rightarrow \infty$ and bin size of $\Delta t \rightarrow 0$ (Paltani 1999), so the characteristic quantities (break timescale and slope) derived from these two methods usually are inconsistent with each other (Kataoka et al. 2001; Zhang et al. 2002).

In blazar timing studies, the variability can also be characterized in terms of excess variance. The variance estimate provides a simple and straightforward means of quantifying the X-ray variability. However, there is a rather large scatter in the variance associated with the stochastic nature of red-noise variability. This implies that only the mean variance averaged from a large number of data sets is meaningful. Previous variance estimates of blazars were usually calculated using only a single light curve (e.g., Zhang et al. 2002; Ravasio et al. 2004). Quantitative comparisons of individual variances estimated in such a way, usually referring to the repeated observations of the same source at different epochs, can be misleading, because an observed light curve is only a single realization of a stochastic red-noise process (Press 1978). Such a comparison is desirable, since one wants to know if the underlying process responsible for the variability evolves with time, i.e., the stationarity of the variability. Only real changes in the variance (or PSD), quantified with the mean variance (or PSD) averaged from a number of light curves or a number of segments of a long light curve, would reflect changes in the physical conditions of the variability process.

Recently, Vaughan et al. (2003b) explored some practical aspects of measuring the amplitude of variability in "red-noise" light curves typical of AGNs. They examined the statistical properties of the quantities commonly used to estimate the variability amplitude in AGN light curves, such as excess variance, $\sigma_{\rm XS}^2$, and the fractional rms variability amplitude, $F_{\rm var}$. Using a long, consecutive *XMM-Newton* light curve, they explored the variability properties of a bright Seyfert 1 galaxy, Mrk 766. The source is found to show a linear correlation between absolute rms variability amplitude and flux and to show significant spectral variability.

In this paper we use variance estimators to examine the variability properties of all public *XMM-Newton* observations for PKS 2155−304 taken over a period of about 3 years (12 exposures from 6 orbits). The EPIC pn data are most suitable for such an analysis because of their high count rates. The observations and the data reduction process are presented in § 2. Section 3 discusses some practical aspects of the variance estimator. The results are presented in § 4 and discussed in § 5. The conclusions are summarized in § 6.

2. THE *XMM-NEWTON* OBSERVATIONS

PKS 2155−304 was observed during six orbits of *XMM-Newton* for about 100 ks each over a period of about 3.5 yr. The source was the target of instrument calibration during four out of the six orbits. In this paper, we concentrate on data obtained with the pn camera that are less affected by photon pileup and have better time resolution. There are a total of 12 pn exposures, each lasting about 40 ks. The pn camera was operated in small window (SW) mode during 10 exposures and in timing (TI) mode during 2 exposures. Different filters (thin, medium, and thick) were used. The properties of each exposure are detailed in Table 1, where an identification number is allocated to each exposure.

All pn data were reprocessed using the *XMM-Newton* Science Analysis System (SAS) version 6.0 and the latest available calibration data. First we checked the high particle background periods caused by solar activity. We computed the hard ($E > 10$ keV) count rate and discarded the time intervals in which the count rate is significantly higher and variable. We then checked the photon pileup for the imaging mode, which is strong for a bright

[1] PSD measurement ideally requires evenly sampled light curves. For a light curve observed with periodic (orbital) gaps, even sampling can be obtained by interpolating gaps, if the gaps comprise only a small fraction of the total light curve, or by binning on either of two timescales: binning on a short timescale, say 256 s, for the duration of one single orbital light curve, and binning on an orbital timescale for the duration of the monitoring (e.g., Zhang et al. 1999, 2002).

source such as PKS 2155−304. We determined the central region to be discarded by using the SAS task `epatplot` on different circular and annular regions of each image. The source data were extracted from rings centered on the source position. The inner radius was determined by photon pileup effects; usually the radius of the central circular region to be discarded is 10″. The outer radius, ranging from 35″ to 40″, was fixed by the position of the source on the chip. The timing mode was not affected by the photon pileup effect, and we extracted the source photons from a region 10 RAWX pixels wide, centered on the brightest strip of the source. In order to minimize the photon pileup effect, only single-pixel events (pattern = 0) with the quality flag = 0 were selected. The background events were extracted from the regions least affected by source photons.

In summary, in the imaging mode, exposures 545-1 and 724 were not significantly affected by photon pileup effects, while other exposures in the imaging mode were influenced by this effect. A high particle background occurred in the middle and the end of exposure 174-2 and at the end of exposures 545-2 and 724. In our analysis, we discard exposures 87-1 and 87-2 because the high particle background occurred throughout the whole exposure. Moreover, we also drop exposure 545-2 due to a calibration problem in the timing mode. Detailed information about high particle background and photon pileup effects is shown in Table 1. The observation during orbit 174 was preliminarily analyzed in Maraschi et al. (2005) and Zhang et al. (2004).

3. RANDOM PROCESS AND VARIANCE ESTIMATORS

Before performing data analysis on the *XMM-Newton* light curves mentioned in § 2, it is useful to review some specific aspects related to a variance analysis of the X-ray variability.

3.1. *Integrated PSD and Variance*

Parseval's theorem (see, e.g., van der Klis 1989; Press et al. 1992) shows that the integral of the PSD between two Fourier frequencies f_1 and f_2 ($f_1 < f_2$) yields the expectation value of the "true" variance due to variations between the corresponding timescales ($1/f_2$ and $1/f_1$),

$$\langle S^2 \rangle = \int_{f_1}^{f_2} \mathcal{P}(f)\, df. \tag{1}$$

An astronomical light curve, usually a discrete time series x_i, is just a realization of a random process, and the integrated periodogram gives rise to the observed variance for that particular realization,

$$S^2 = \sum_{j=1}^{N/2} P(f_j)\Delta f, \tag{2}$$

where Δf is the frequency resolution of the discrete Fourier transform (DFT) for the discrete time series [$\Delta f = 1/(N\Delta T)$, where ΔT is the bin size of the light curve]. The total variance of a real light curve is equal to its periodogram integrated from the frequency range $f_1 = 1/(N\Delta T)$ to $f_{\rm Nyq} = 1/(2\Delta T)$ (the Nyquist frequency). It is important to note that the periodogram $P(f_j)$ is only one realization of the underlying $\mathcal{P}(f)$.

The observed variance can be simply obtained from the light curve:

$$S^2 = \frac{1}{N-1}\sum_{i=1}^{N}(x_i - \bar{x})^2, \tag{3}$$

where $\bar{x}$ is the arithmetic mean of x_i. This variance is usually different from observation to observation (see discussion below). In the limit of large N, the variance estimate from the light curve should be identical to the one integrated from the corresponding periodogram.

Equation (3) also indicates that the variance is proportional to the square of the count rate. For example, if the count rate obtained from a detector (e.g., *XMM-Newton* pn) is a factor of m larger than the one simultaneously obtained from another detector (e.g., *XMM-Newton* MOS1 or MOS2), the variance obtained from the former detector is a factor of m^2 larger than the one simultaneously obtained with the latter detector. However, this does not imply that the source variability is different from the two detectors at the same time. Therefore, in order to compare the variance obtained from different detectors or from the observations at different epochs or between different sources, the normalized variance, $S^2/\bar{x}^2$, is usually used.

3.2. *Excess Variance and $F_{\rm var}$*

A real light curve x_i has finite uncertainties σ_i due to measurement errors (Poisson noise for an X-ray photon counting signal). The uncertainties due to photon counting also yield an additional variance that should be subtracted in order to obtain the *intrinsic* variance. This is the so-called excess variance (Nandra et al. 1997; Edelson et al. 2002),

$$\sigma_{\rm XS}^2 = S^2 - \overline{\sigma^2}, \tag{4}$$

where $\overline{\sigma^2}$ is the mean error squared,

$$\overline{\sigma^2} = \frac{1}{N}\sum_{i=1}^{N}\sigma_i^2. \tag{5}$$

Here $\sigma_{\rm XS}^2$ is an absolute quantity that linearly correlates with the count rate. Because the count rates are independent, the normalized excess variance, simply given by $\sigma_{\rm NXS}^2 = \sigma_{\rm XS}^2/\bar{x}^2$, is often used for comparing variances between different observations (or different segments of a long observation) of the same source and between different sources. The square root of $\sigma_{\rm NXS}^2$ is the fractional rms variability amplitude, $F_{\rm var}$, a common measure of the intrinsic variability amplitude that corrects the effects of the measurement errors (Edelson et al. 1990; Rodríguez-Pascual et al. 1997):

$$F_{\rm var} = \sqrt{\frac{S^2 - \overline{\sigma^2}}{\bar{x}^2}}. \tag{6}$$

3.3. *Intrinsic Scatter in Variance*

Since red-noise variability is a stochastic process, one should expect random fluctuations in both the mean and the variance with time (between segments of a long observation or between observations taken at different epochs). For a stationary process whose statistical properties do not evolve with time, the distribution of the individual variances from red noise with a steep PSD has a non-Gaussian shape with rather large scatter (Vaughan et al. 2003b). This scatter is intrinsic to the stationary process, which is caused by the limited length of a given observation. This means that the red-noise variability is weakly nonstationary (Press & Rybicki 1997). Thus, the scatter in the variance is not caused either by the measurement errors or by the number of data points used. However, the underlying process responsible for the variability itself may also change with time (e.g., if the PSD and variance change with time). If this is the case, the variability is said to be strongly nonstationary. Real changes in the variability

process could provide insight into the changing physical conditions in the nuclear emission region, while the random changes of statistical moments expected for a stationary red-noise process yield no physical insight. As the purpose of timing series analysis is to gain insight into the physical process, it is desirable to discriminate the changes in variance produced by a time-stationary process and by a strong nonstationary process. Therefore, all the subsequent nonstationarity discussed hereafter throughout the text refers to strong nonstationarity.

The stochastic nature of a red-noise process implies that only the mean properties of the statistical quantities averaged from a number of data sets can provide physical insight. Averaging over many independent realizations reduces the random fluctuations inherent in the red-noise process. The expectation values, rather than one realization, of the statistical quantities (such as variance) should be representative of the properties of the underlying process. In order to search for nonstationary variability, an ensemble of light curves (or of short segments of a long light curve) is therefore needed. For example, comparing different PSDs is the method frequently employed in the timing analysis of X-ray binaries. The mean PSDs averaged from the periodograms of a large number of light curves show significant differences from epoch to epoch, indicating that the variability process of X-ray binaries is strongly nonstationary (e.g., van der Klis 1995). Moreover, even more important is the way in which the variability properties evolve with time, from which one can effectively infer the detailed working mechanisms in these systems (e.g., Belloni & Hasinger 1990; Uttley & McHardy 2001; Belloni et al. 2002; Pottschmidt et al. 2003).

However, unlike X-ray binaries, AGN data are usually not adequate for performing a full PSD analysis. In order to search for nonstationarity of the variability in a number of short light curves (or of short segments of a long light curve), one can test whether the variances differ significantly. Vaughan et al. (2003b) proposed three practical methods as variance estimators. (1) The individual variance estimates are compared with the expected scatter around the mean. Here the expected scatter is calculated using Monte Carlo simulations of a stationary processes. Because the intrinsic scatter in the variance of a stationary process is rather large for red-noise data, this method is only sensitive to very large changes in the variability amplitude. Moreover, one has to assume a PSD shape for the analyzed source. (2) The variances are averaged at various epochs by binning a number ($N \geq 20$) of individual variance estimates. Here the light curve segments from which the individual variance are calculated should have the same sampling properties in bin size, length, and number of data points. This is most useful when searching for subtle changes in variability amplitude but requires large data sets (in order that the variance can be sufficiently averaged). (3) Individual variance estimates can be sorted and binned by count rates so that a relationship between the variance or $F_{\rm var}$ and the count rate can be constructed. The existence of a correlation would imply that the variability process is strongly nonstationary, as the random fluctuations in variance should not produce such a correlation. A linear correlation between binned, absolute rms variability amplitude and flux has been found in X-ray binaries and Seyfert galaxies, indicating nonstationarity of the X-ray variability (Uttley & McHardy 2001).

4. RESULTS

4.1. *Changes of the XMM-Newton Light Curves*

The background-subtracted, 25 s binned, broadband 0.2–10 keV light curves extracted from the pn camera are shown in Figures 1–5 (*panel 1*). The length of the observation for a full revolution (i.e., revolutions 174, 362, 450, and 545) is about 10^5 s. The source showed significant variability during each revolution, but unfortunately, no complete flares were obtained due to the interruption of the observations. It is likely that a pronounced flare occurred at the beginning of revolution 362 and at the end of revolution 450. The observations also showed that the variability of PKS 2155−304 (and Mrk 421; Brinkmann et al. 2003; Ravasio et al. 2004) is dominated by somewhat smooth flares rather than by rapid "flickers" in the X-ray light curves typical of Seyfert 1 galaxies, e.g., the *XMM-Newton* light curves of MCG −6-30-15 (Vaughan et al. 2003a) and Mrk 766 (Vaughan et al. 2003b). Such qualitative differences in the X-ray light curves may reflect the different mechanisms producing the variability in the two classes, i.e., TeV blazars are jet-dominated systems while Seyfert 1 galaxies are disk-dominated systems. It further indicates that the PSD slopes of TeV blazars might be steeper than those of Seyfert 1 galaxies.

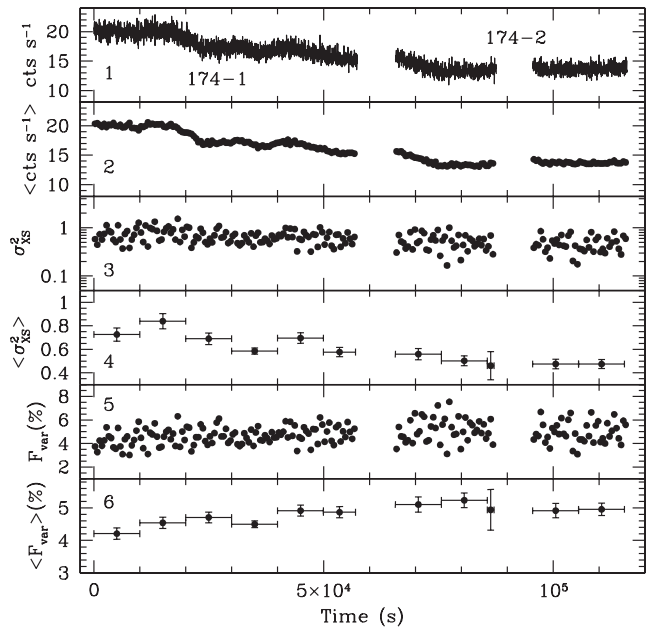

FIG. 1.—*Panel 1*: Background-subtracted, 25 s binned, 0.2–10 keV pn light curve of PKS 2155−304 obtained in revolution 174. Note that there is a small offset of the count rate between 174-1 and 174-2 due to different extraction regions of the source photons. A high particle background occurred in the middle and the end of 174-2. *Panels 2 and 3*: Mean count rate and excess variance, calculated from 20 consecutive points of panel 1. Panel 2 corresponds to the light curve binned over 500 s. *Panel 4*: Mean excess variance, averaged by binning 20 continuous individual excess variances. This average excess variance is inconsistent with a constant. *Panel 5*: Fractional rms variability amplitude, calculated from 20 continuous points of panel 1. *Panel 6*: Mean fractional rms variability amplitude, averaged by binning 20 continuous individual amplitudes. This average fractional rms variability amplitude is also inconsistent with a constant.

In order to test the stationarity of the light curves, we calculated the mean count rate and the excess variance for every 20 consecutive data points in the light curves. This corresponds to "instantaneous" estimates of the source variance over a timescale of 50–500 s. The results are shown in panels 2 and 3 of Figures 1–5. Panel 2 corresponds to the light curve binned over a timescale of 500 s. As expected for red-noise variability, the individual source variances (*panel 3*) show large changes within each revolution. The expected range for the excess variance and the normalized excess variance, calculated using the simulation results (Table 1 of Vaughan et al. 2003b) under the assumption

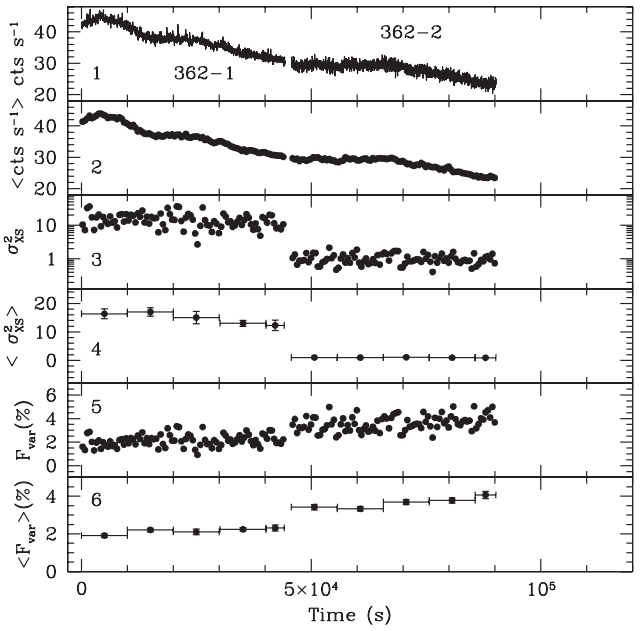

FIG. 2.—Same as Fig. 1, but using the light curve obtained during revolution 362. *Panel 1*: The count rates of 362-1 (timing mode) were scaled down by a factor of 4.7 in order to smoothly connect with those of 362-2 (imaging mode). *Panel 4*: The average excess variance of 362-1 is inconsistent with a constant. *Panel 6*: The average fractional rms variability amplitude is also inconsistent with a constant.

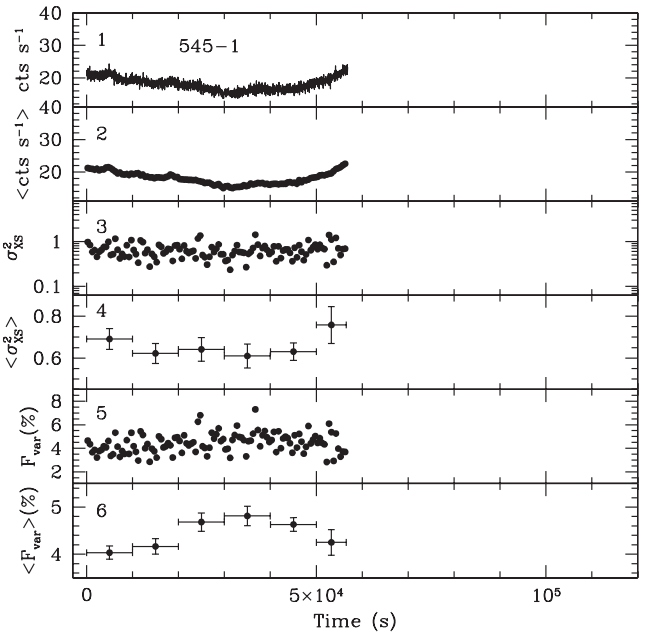

FIG. 4.—Same as Fig. 1, but using the light curve obtained during revolution 545. Only 545-1 data are shown; 545-2 data are not shown due to a calibration problem. *Panel 6*: The average fractional rms variability amplitude is inconsistent with a constant.

of a PSD slope $\alpha = 2.0$, is plotted in Figures 6–9. Normalized excess variance, corresponding to the individual $F_{\rm var}$ estimates in panel 5 of Figures 1–5, can be compared for different exposures of each revolution (and of different revolutions). Neither of these figures show fluctuations of source variance larger than the range expected for a stationary red-noise process. Note that the confidence ranges marked here should be considered approximate values, since the PSD slope of PKS 2155−304 is probably larger than 2 (e.g., Zhang et al. 2002), yielding larger confidence ranges. These tests are consistent with the variability of PKS 2155−304 being a stationary process. As stated before, however, the real changes of source variances may be masked by the rather large scatter in variance expected for stationary red-noise variability.

Subtle changes in the variability amplitude can be identified by calculating the mean variance and its error through

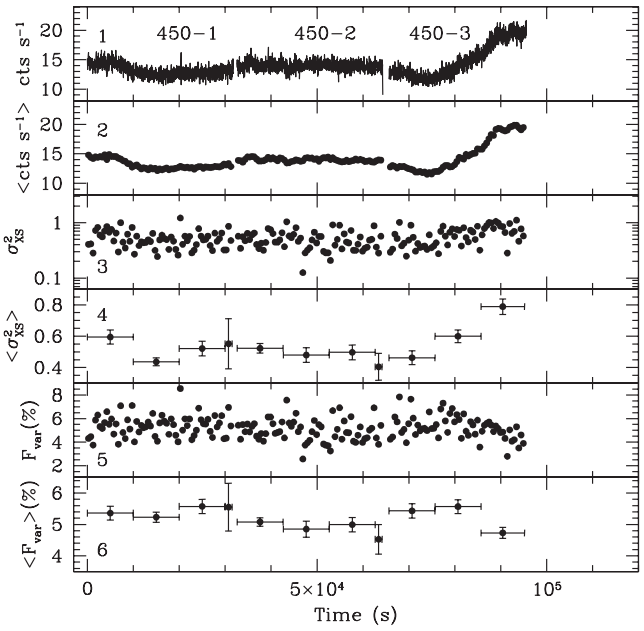

FIG. 3.—Same as Fig. 1, but using the light curve obtained during revolution 450. Due to the different filters and extraction regions used for each exposure, there are small offsets of count rates between different exposures. *Panel 4*: The average excess variance of 450-1 and 450-3 is inconsistent with a constant. *Panel 6*: The average fractional rms variability amplitude of 450-3 is also inconsistent with a constant.

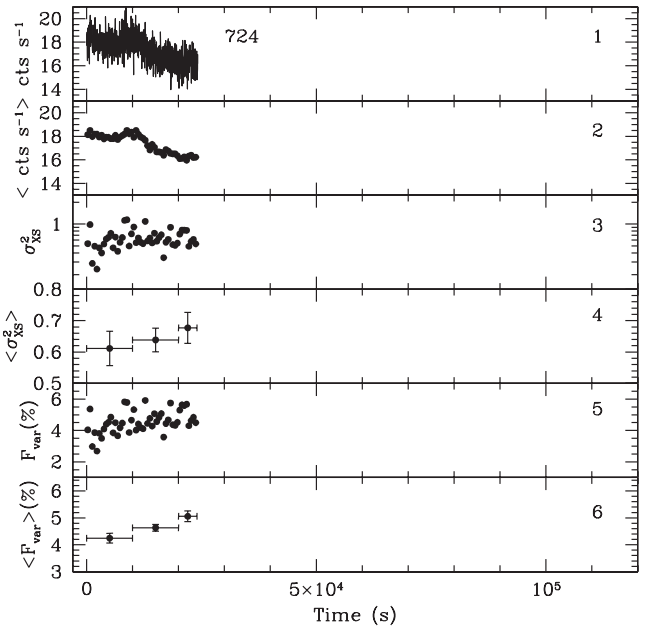

FIG. 5.—Same as Fig. 1, but using the light curve obtained during revolution 724. A high particle background occurred in the end of this observation. *Panel 6*: The average fractional rms variability amplitude is inconsistent with a constant. Due to the short observation length, we do not discuss it in the text.

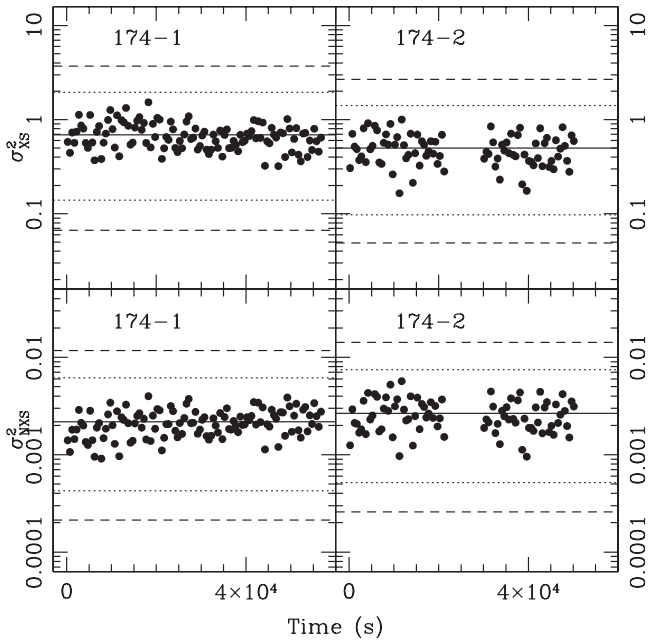

FIG. 6.—Excess variance (*top*) of PKS 2155−304, same as that shown in panel 3 of Fig. 1, and the corresponding normalized excess variance (*bottom*). The solid line marks the mean variance, and the dotted and dashed lines mark the 90% and 99% confidence intervals around the mean, respectively. The variances fall within the limits, as expected for a stationary process.

binning the consecutive individual variance estimates. The *XMM-Newton* data of PKS 2155−304 are sufficient to examine changes of the average variance with time, allowing us to perform a more sensitive test for nonstationarity of the variability. We calculated the mean excess variance by binning 20 consecutive individual excess variance estimates and assigning an error bar using equation (4.14) of Bevington & Robinson (1992). The results are shown in panel 4 of Figures 1–5. Significant changes in the average variance with time are revealed for exposures

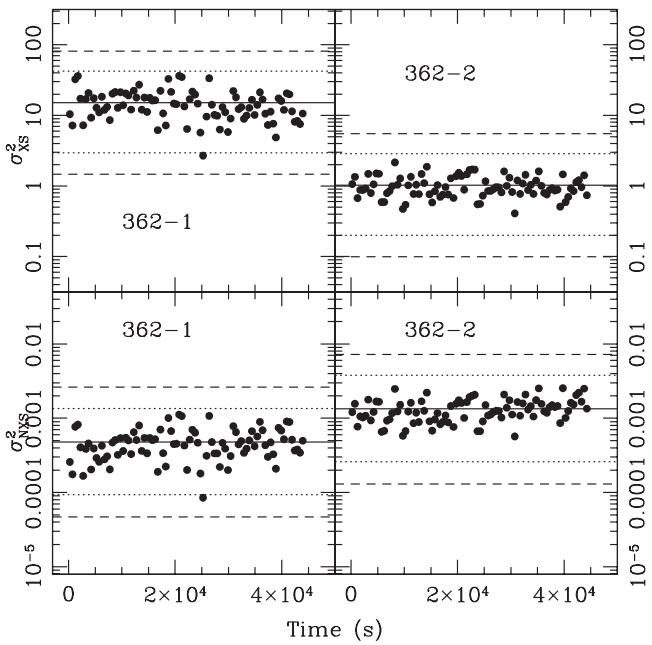

FIG. 7.—Same as Fig. 6, but using data from revolution 362. The variances fall within the limits, as expected for a stationary process.

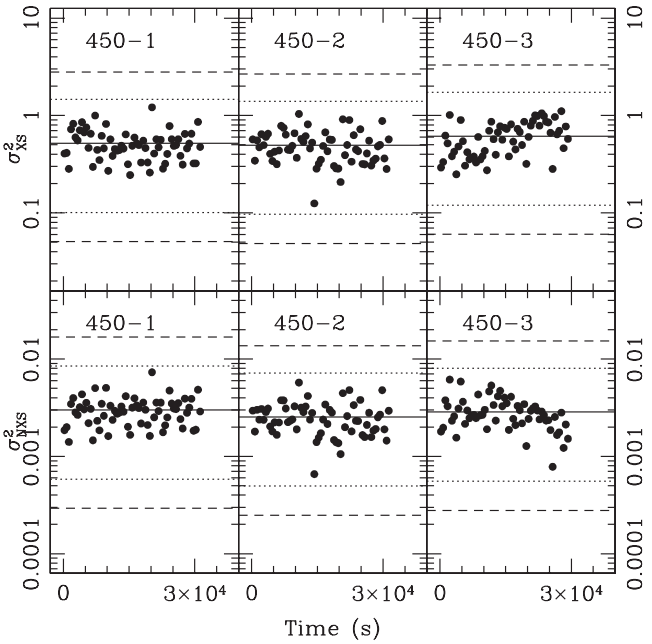

FIG. 8.—Same as Fig. 6, but using data from revolution 450. The variances fall within the limits, as expected for a stationary process.

174-1, 362-1, 450-1, and 450-3, in which the source showed significant variations. In order to test the significance of such changes, we fitted the mean variance with a constant for each exposure. The fitting can be rejected at larger than 95% confidence for exposures 174-1 ($\chi^2 = 21.2$ for 5 degrees of freedom [dof]), 450-1 ($\chi^2 = 10.2$ for 3 dof), and 450-3 ($\chi^2 = 24.2$ for 2 dof) and at 90% confidence for exposure 362-1 ($\chi^2 = 7.6$ for 4 dof), indicating that the mean excess variance is not consistent with a constant hypothesis, i.e., the average excess variance changes with time. For other exposures, the changes in the mean variance are consistent with a constant hypothesis due to small variations or short exposure length. The results indicate

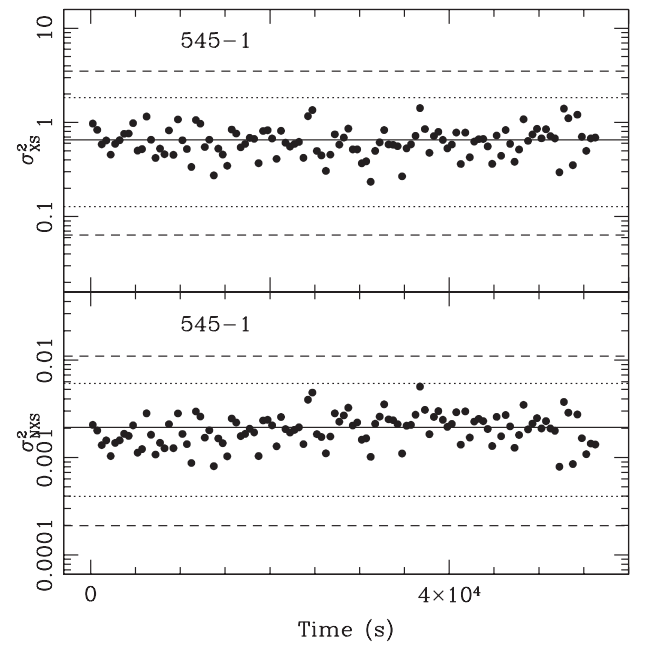

FIG. 9.—Same as Fig. 6, but using data from revolution 545-1. The variances fall within the limits, as expected for a stationary process.

that the variability of PKS 2155−304 tends to be nonstationary during flare states.

To compare variability amplitude in different exposures, we further calculated $F_{\rm var}$ and its average in the same way as the excess variance. Panels 5 and 6 of Figures 1–5 show individual $F_{\rm var}$ estimates and their averages as a function of time. Each point of $F_{\rm var}$ and its average corresponds to that of each $\sigma_{\rm XS}^2$ and its average. The fitting with a constant showed that the mean $F_{\rm var}$ is inconsistent with a constant at larger than 95% confidence for exposures 174-1, 362-1, 362-2, 450-3, 545-1, and 724. Therefore, our analysis shows that the variability of PKS 2155−304 does show genuine nonstationarity in the sense of both the absolute and the fractional variability amplitude (i.e., $\sigma_{\rm XS}^2$ and $F_{\rm var}$).

4.2. *Flux–rms Correlations*

Figures 1–5 (*panels 4 and 6*) show that the mean $\sigma_{\rm XS}^2$ and $F_{\rm var}$ have a tendency to track the mean count rate, but in an opposite sense: $\sigma_{\rm XS}^2$ tends to increase, while $F_{\rm var}$ tends to decrease, with an increasing count rate. This trend is difficult to discern from the individual $\sigma_{\rm XS}^2$ and $F_{\rm var}$ estimates (panels 3 and 5 of Figs. 1–5) due to large scatter.

In order to quantify the dependence of excess variance on the count rate, we sorted individual excess variance estimates by the count rate and binned $\sigma_{\rm XS}^2$ every 20 estimates. The error on the mean $\sigma_{\rm XS}^2$ was calculated in the standard way as detailed above. The results are shown in Figures 10–13 (*top*), where the mean absolute rms amplitude [i.e., the square root of the excess variance, $(\sigma_{\rm XS}^2)^{1/2}$] is shown as a function of the mean count rate. These figures clearly show that the absolute variability amplitude correlates linearly with the flux. The offsets of count rates for the different exposures of revolutions 174 and 450 are negligible, so we put them in a single plot. The source therefore does show strong nonstationarity: the absolute variability amplitude increases, on average, as the source flux increases. This kind of correlation has been noted in X-ray binaries and in Seyfert galaxies (Uttley & McHardy 2001; Edelson et al. 2002; Vaughan et al. 2003a) and is due to a linear correlation between rms and flux (see also § 3.1). This effect therefore may not imply real nonstationarity of the variability. Panels 3 and 4 of Figure 2 clearly demonstrate this: the excess variances of 362-1 are systematically about 1 order of magnitude larger than those of 362-2, because exposure 362-1 was obtained in pn timing mode, while 362-2 was obtained in pn imaging mode. In Figure 2, the count rates of 362-1 were scaled down by a factor of about 5 in order to smoothly connect with those of 362-2. We

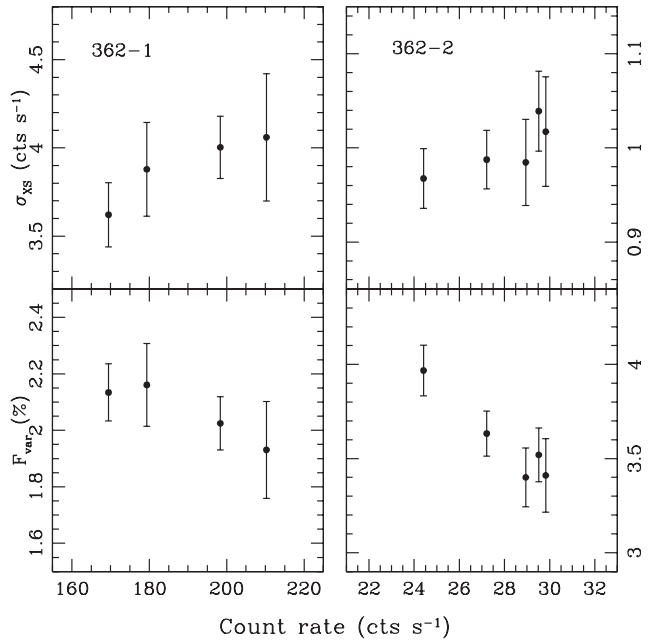

FIG. 11.—Same as Fig. 10, but using data from revolution 362. For both exposures, the absolute rms variability amplitude correlates with flux, but the fractional rms variability amplitude anticorrelates with flux.

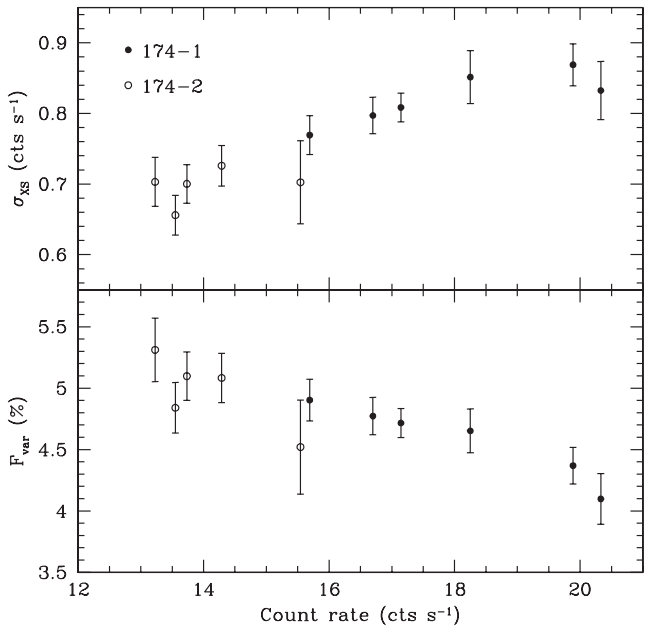

FIG. 10.—Mean absolute rms variability amplitude [$\sigma_{\rm XS} = (\sigma_{\rm XS}^2)^{1/2}$; *top*] and mean fractional rms variability amplitude ($F_{\rm var}$; *bottom*) as a function of count rate. Clearly, the absolute rms amplitude correlates with flux, but the fractional rms amplitude anticorrelates with flux. The small offset of count rates between different exposures does not alter such correlations.

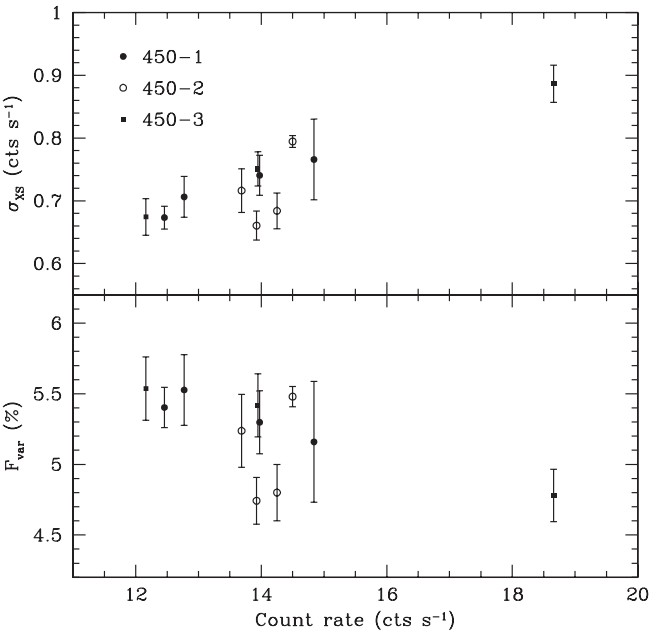

FIG. 12.—Same as Fig. 10, but using data from revolution 450. Clearly, the absolute rms variability amplitude correlates with flux, but the fractional rms variability amplitude anticorrelates with flux. The small offset of count rates between different exposures does not alter such correlations.

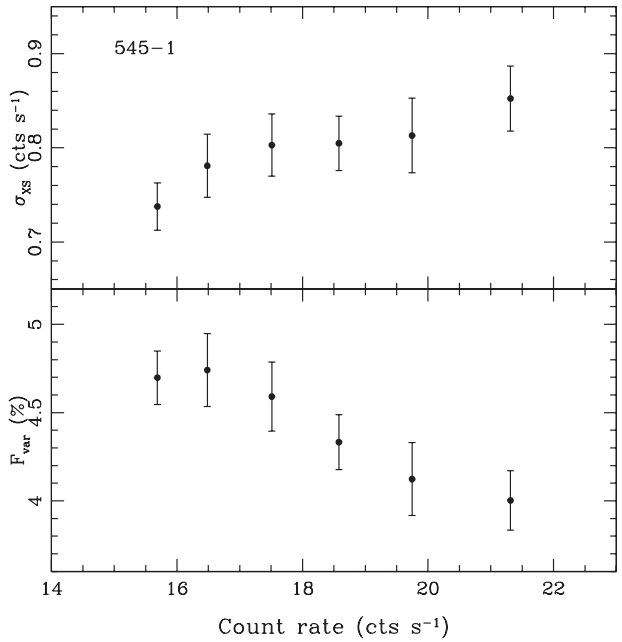

FIG. 13.—Same as Fig. 10, but using data from revolution 545-1. Clearly, the absolute rms variability amplitude correlates with flux, but the fractional rms variability amplitude anticorrelates with flux.

can also demonstrate this effect by comparing excess variances of 362-1 with those of 174-1 and 450-3 (panels 3 and 4 of Figs. 1–3). The three exposures show similar variability amplitudes (about a factor of 2 difference from minimum to maximum count rate), but the excess variances of 362-2 were about 1 order of magnitude larger than those of both 174-1 and 450-3.

Normalized variability amplitude ($F_{\rm var}$ or $\sigma^2_{\rm NXS}$) can "filter" such linear correlations. Figures 10–13 (*bottom*) show the binned $F_{\rm var}$ as a function of the mean count rate, which was calculated in the same way as binned $\sigma^2_{\rm XS}$. Interestingly, $F_{\rm var}$ linearly anticorrelates with count rate for all observations, in contrast to the linear correlation between $\sigma^2_{\rm XS}$ and count rate. Therefore, the variability of PKS 2155−304 does show genuine (strong) nonstationarity in the sense that the absolute rms (the excess variance) linearly increases with flux, but the fractional rms (the normalized excess variance or $F_{\rm var}$) linearly decreases with flux. The mean $F_{\rm var}$ is therefore inconsistent with a constant for both time and flux. However, given the small range of flux and variance changes, it is inadequate to determine and compare the slopes of the rms–flux relation and the $F_{\rm var}$-flux relation for each observation. It is also important to point out that the rms–flux relations seen here are consistent with being linear, but the data are not adequate enough to rule out a power-law (nonlinearity) rms–flux relation (see Appendix D of Uttley et al. 2005).

Given the implied steep PSD slopes of PKS 2155−304, a red-noise leak may be contaminating the variability amplitudes. The variability amplitude of a light curve that is a realization of a red-noise process may be dominated by trends on timescales much longer than the duration (500 s) considered here. This may especially be true for blazars during their flare states, where smooth increases or decreases in flux over tens of kiloseconds may contribute greatly to a variability amplitude measured on time scales of 500 s and shorter. If the dominant flux trends associated with flares are steeper toward higher fluxes (the light curves of PKS 2155−304 seem flatter when the source is not flaring, for instance), this could potentially artificially produce a positive rms–flux correlation. Variability trends on timescales longer than 500 s should be removed from each segment (500 s long) before measuring the variability amplitude. For each segment, we did a least-squares fit to find the best-fitting line to characterize the overall dominating increasing or decreasing trend, subtracted the trend from the flux points, and then measured the excess variance and $F_{\rm var}$ again. This yielded values of the excess variance that were only about a few percent smaller than the previous values (without "detrending"), since the variability contributions from the red-noise leak were removed. However, this detrending did not change the flux–rms relation and the flux-$F_{\rm var}$ relation. Therefore, the red-noise leak does not significantly affect the excess variance and the $F_{\rm var}$ calculated between 25 and 500 s. Furthermore, the steep PSD slope indicates that the intrinsic variability of the source is expected to be quite low at high temporal frequencies. We thus measured an unbinned periodogram for each light curve with a resolution of 10 s. The results showed that the intrinsic variability of the source is indeed much greater than the white noise variability due to Poisson noise on temporal frequencies between 0.002 Hz (1/500 s) and 0.02 Hz (1/50 s).

4.3. *Root Mean Squared Spectra*

The dependence of the variability amplitude on photon energy can, in principle, reveal the spectral variability of a source. This dependence is called the rms spectrum because the variability amplitude is measured with the common fractional rms variability amplitude, $F_{\rm var}$ (e.g., Edelson et al. 2002; Vaughan et al. 2003b). A rms spectrum quantifies how the variability changes with photon energy. If $F_{\rm var}$ (or normalized excess variance) is found to change significantly from one energy band to another, the PSD (slope or amplitude) must be energy-dependent. The changes of the variability amplitude with energy have been noted before in Mrk 421 and PKS 2155−304: the sources are systematically more variable toward higher energy (e.g., Fossati et al. [2000] and Zhang et al. [1999, 2002] with *BeppoSAX* data and Edelson et al. [2001], Sembay et al. [2002], and Ravasio et al. [2004] with *XMM-Newton* data).

However, given the length and the bin size of a light curve, $F_{\rm var}$ measures the integrated variability amplitude (see § 3.1). As TeV blazars (AGNs in general) have steep "red-noise" PSDs (e.g., Kataoka et al. 2001; Zhang et al. 2002), $F_{\rm var}$ is dominated by variations on the longest timescales probed by that light curve (e.g., Markowitz & Edelson 2001). In order to probe short-timescale variability we use a related parameter, called point-to-point fractional rms variability amplitude ($F_{\rm pp}$; Edelson et al. 2002),

$$F_{\rm pp} = \frac{1}{\bar{x}} \sqrt{\frac{1}{2(N-1)} \sum_{i=1}^{N-1} (x_{i+1} - x_i)^2 - \overline{\sigma^2}}. \qquad (7)$$

Here $F_{\rm pp}$ measures the variations between adjacent points (the sum of the squared difference of count rates between adjacent points, minus the effects of measurement errors, and normalized by mean count rate). For white noise, $F_{\rm pp}$ and $F_{\rm var}$ are identical. However, for red-noise variability, $F_{\rm var}$ is larger than $F_{\rm pp}$, because the variations are larger on longer timescales. The spectra of $F_{\rm var}$ and $F_{\rm pp}$ measure the energy dependence of the variability at long and short timescales, respectively, so the ratio of $F_{\rm var}$ to $F_{\rm pp}$ as a function of energy can, in principle, reveal the dependence of the PSD slope on energy: the larger the ratio, the steeper the PSD slope. If the ratio is energy-independent, the PSD slope is then energy-independent.

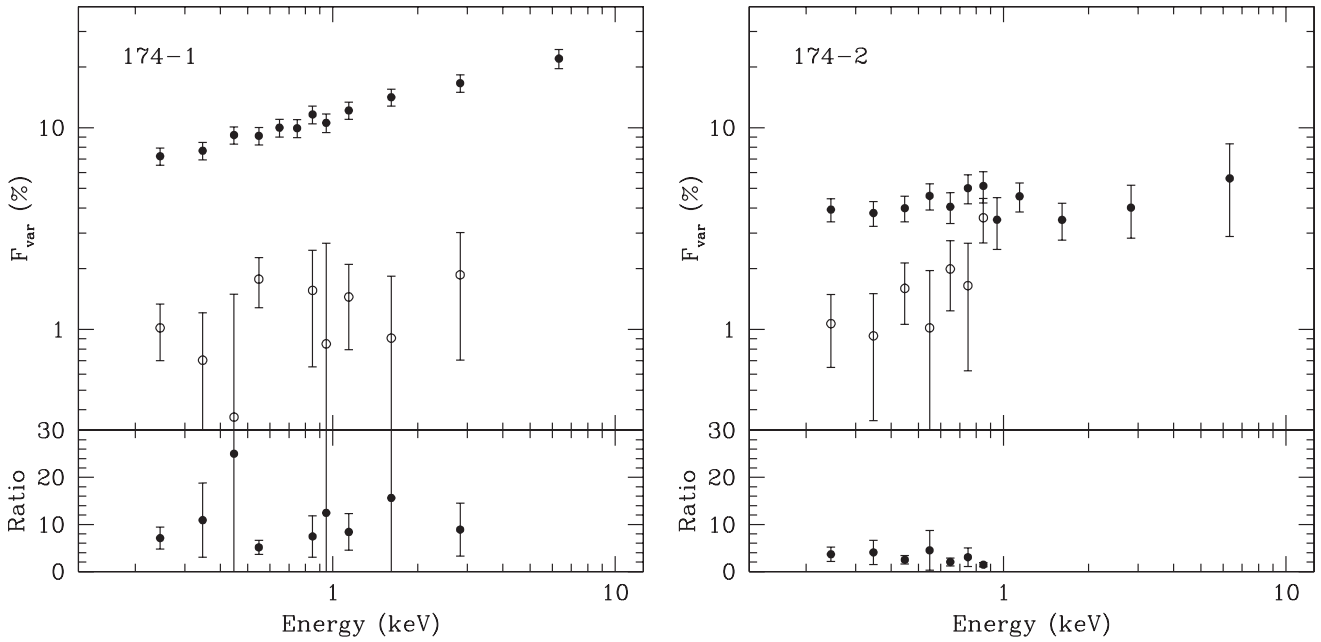

FIG. 14.—*Top*: Fractional rms variability amplitude vs. energy on two different timescales. The upper spectrum shows the variability amplitude integrated over timescales between the exposure length and 2000 s. Because of the red-noise variability, this spectrum is dominated by variations on timescales comparable to the length of the exposure. The lower spectrum represents the rms deviation between neighboring points (i.e., point-to-point rms), sampling variability only on short timescales (∼1000 s). *Bottom*: Ratio of the two rms spectra (i.e., the ratio spectrum). The ratio spectrum shows the way that the energy dependence of the variability amplitude changes with variability timescales, qualitatively representing the energy dependence of PSD. The errors were derived as described in the text.

We split the light curve extracted from each exposure into 12 different energy bands (0.2–0.3, 0.3–0.4, 0.4–0.5, 0.5–0.6, 0.6–0.7, 0.7–0.8, 0.8–0.9, 0.9–1, 1–1.3, 1.3–2, 2–4, and 4–10 keV). The light curves in each band are then binned over 1000 s. They are strictly simultaneous and continuous, except for 174-2 (there is a long gap due to high particle background). For each light curve, we calculated F_{var} and F_{pp} spectra and their ratio spectra. The errors of F_{var} and F_{pp} were calculated using equation (2) of Edelson et al. (2002), and the error for the ratio was propagated from the errors on F_{var} and F_{pp}. The errors on F_{var} and F_{pp} should be considered conservative estimates of the true uncertainty, since they strictly assume that the light curves are drawn from independent Gaussian processes.

The upper spectrum of Figures 14–17 shows the F_{var} spectrum, the fractional rms variability amplitude integrated between the entire observation length and the Nyquist frequency (2000 s or 5×10^{-4} Hz), i.e., over about 1 order of the Fourier frequency range. This frequency range mostly has gaps determined by the periods of low–Earth orbital satellites such as *BeppoSAX* (Zhang et al. 2002). Since the variability is dominated by the longest timescale of a given exposure, the F_{var} spectrum therefore reveals the energy dependence of the variations occurring

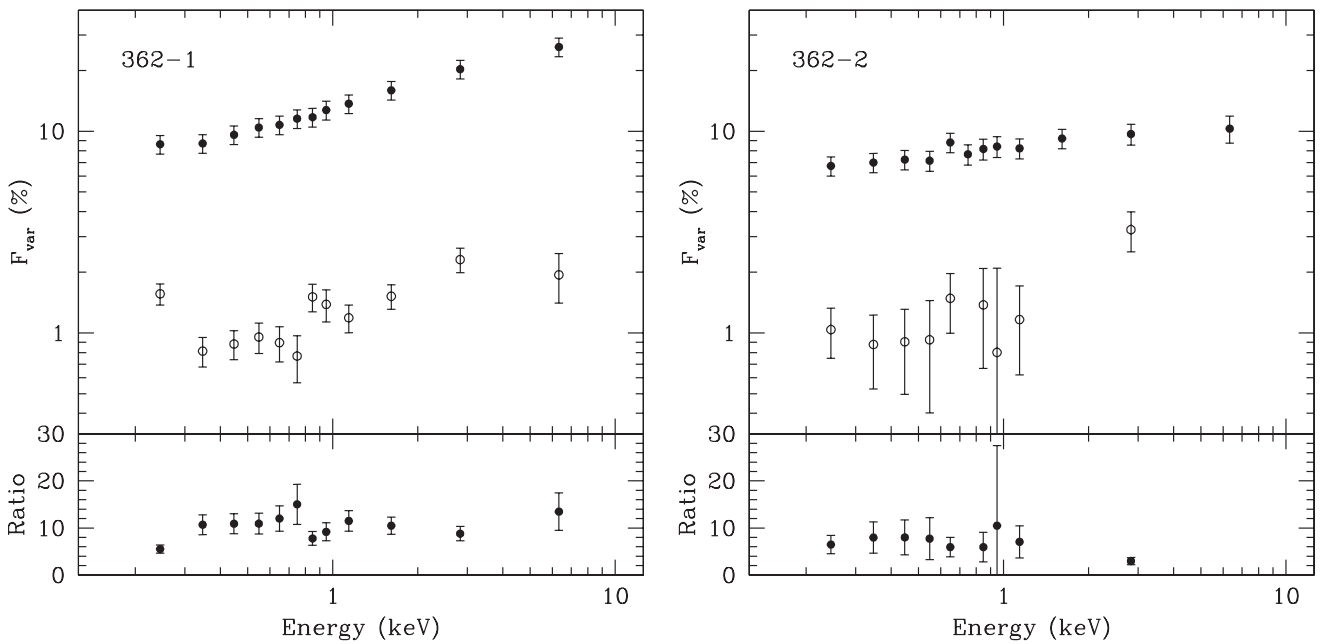

FIG. 15.—Same as Fig. 14, but using data from exposures 362-1 and 362-2.

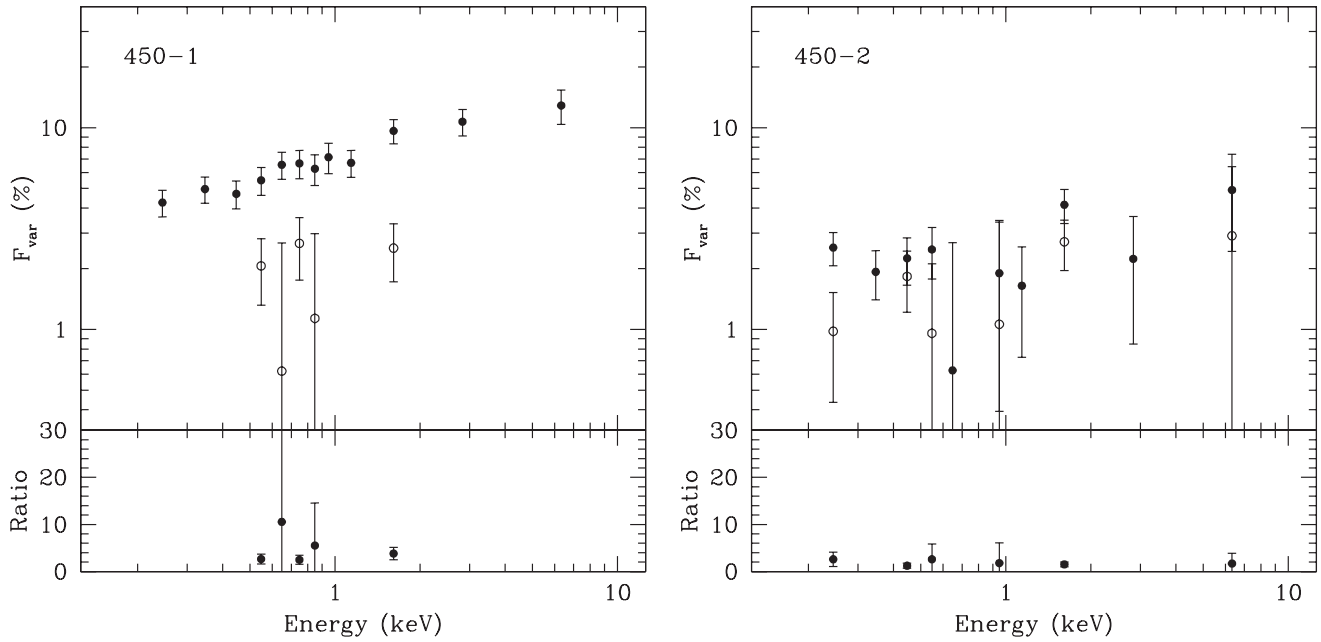

FIG. 16.—Same as Fig. 14, but using data from exposures 450-1 and 450-2.

on timescales comparable to the exposure length ($\sim 4 \times 10^4$ s). It is clear from the figures that the F_{var} spectra of PKS 2155−304 strongly depend on the energies during flare states (i.e., 174-1, 362-1, 450-3, and 545-1), in the sense that the variability amplitude logarithmically increases with increasing energy. This trend indicates that the source experienced strong spectral variability during its active states. The F_{var} spectrum of 450-1 also clearly depends on the energy, but the variability amplitude is relatively small. The dependence of the variability amplitude on the energy is marginal for 362-2. The F_{var} spectra of 174-2 and 450-2 were poorly determined and do not show clear energy dependence when the source was least variable. Moreover, it seems that the slope of such dependence differs from observation to observation. The results show that the variability of PKS 2155−304 strongly depends on the energy during flare periods, while such dependence become marginal or even disappears when the source is less variable or in a quiet state. This phenomenology was previously found in the *BeppoSAX* data of Mrk 421 (Fossati et al. 2000). It is worth pointing out that the sampling of the *XMM-Newton* light curves used here are consecutive, without gaps (except for 174-2).

The lower spectrum of Figures 14–17 shows the F_{pp} spectrum, measuring fluctuations between neighboring points and so probing the energy dependence of the variability on short timescales comparable to the bin size ($\sim$1000 s). However, the F_{pp} spectra were poorly measured due to small variations of the source on short timescales. In fact, in some cases the values of F_{pp}^2 are negative due to large measurement errors; therefore,

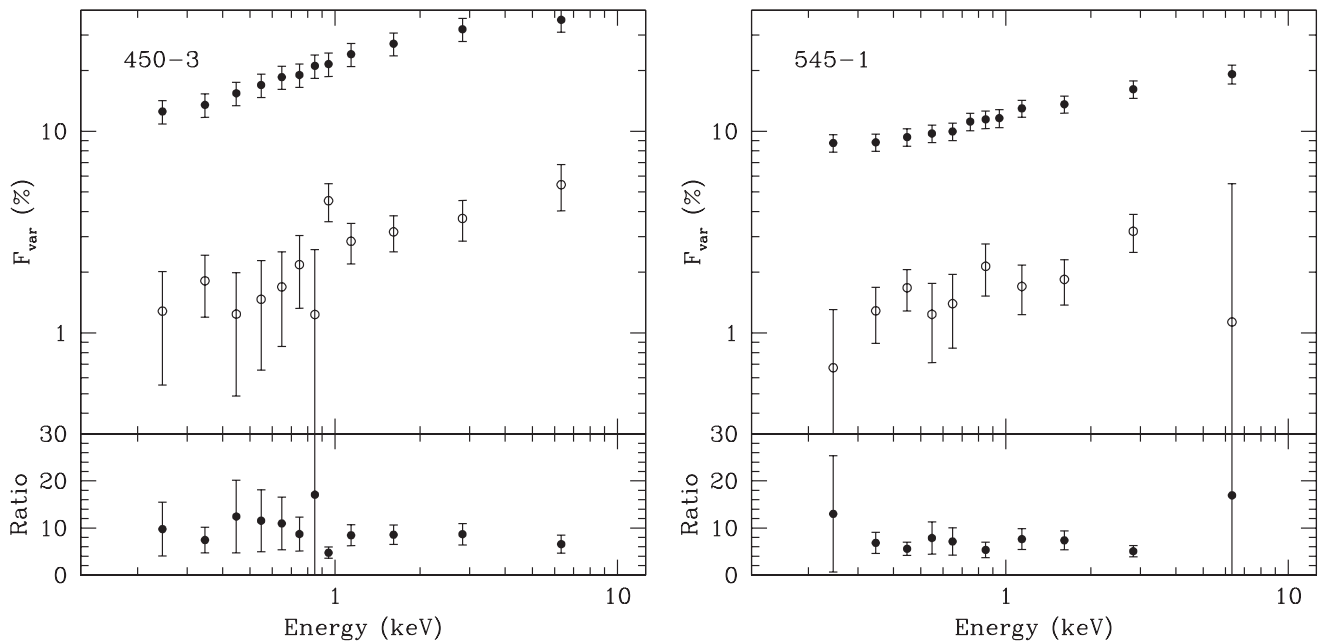

FIG. 17.—Same as Fig. 14, but using data from exposures 450-3 and 545-1.

these points are not present in the F_{pp} spectra of Figures 14–17. It is interesting to note that in some cases (e.g., 450-3) in which the F_{pp} spectrum was relatively well determined, the F_{pp} spectrum tends to track the trend of the F_{var} spectrum, suggesting that the ratio spectra of F_{var} to F_{pp} is energy-independent. One can see from Figures 14–17 that the ratio spectra do not show significant features, mostly keeping constant with energy. This further indicates that the PSD slope of PKS 2155−304 is possibly energy-independent, but the PSD amplitude should be energy-dependent, as the F_{var} spectrum is energy-dependent in the sense that the PSD amplitude is larger for higher energy. This phenomenology has been noted in the *XMM-Newton* observations of Mrk 421 by directly comparing the PSDs in the soft and hard energy bands (see Fig. 20 of Brinkmann et al. 2003).

4.4. *Estimate of Black Hole Mass*

The variability amplitude of AGNs in terms of σ^2_{NXS} or PSD amplitude at a given timescale (or temporal frequency) anticorrelates with the source luminosity (Nandra et al. 1997; Turner et al. 1999; Leighly 1999; Markowitz & Edelson 2001), and with the central black hole mass (M_{BH}) of AGNs (Bian & Zhao 2003). The long, well-sampled *RXTE* light curves of a few Seyfert 1 galaxies revealed an unambiguous characteristic "break frequency," ν_{bf}, at which the PSD changes in slope from 2 above to 1 below (Uttley et al. 2002; Markowitz et al. 2003). The break frequencies of Seyfert 1 galaxies are thought to be analogous to those of black hole X-ray binaries (BHXRBs) in a high state or the high-frequency break of BHXRBs in a low state. The break frequency, at which the PSD changes slope from 2 above to 1 below, appears to anticorrelate with M_{BH} from AGNs to BHXRBs, with the relationship $1/\nu_{bf} \propto M_{BH}$ (Uttley et al. 2002; Markowitz et al. 2003; Papadakis 2004). This is known as the linear scaling law of the PSD parameters with M_{BH} between AGNs and BHXRBs. However, the PSD break timescale–M_{BH} scaling relation of Markowitz et al. (2003) & McHardy et al. (2004) is consistent with being linear, but the slope is in fact poorly constrained (if Cyg X-1 is not taken into account).

The break frequency more accurately represents the underlying dynamical process of the source. The relation $1/\nu_{bf} \propto M_{BH}$ can therefore be used to infer M_{BH} in AGNs by taking the M_{BH} of Cyg X-1 as a reference point. This method, however, requires an unambiguous determination of ν_{bf} in the AGNs, which was impossible before *RXTE*. Instead, Hayashida et al. (1998) and Czerny et al. (2001) used the normalized PSD to estimate the M_{BH} for AGNs by calculating the ratio of the frequencies at which $f\mathcal{P}(f)$ has a certain (well defined) value for both the AGNs and Cyg X-1. However, this method still requires rather long, high-quality data that are available only for a few AGNs.

Equation (1) indicates that σ^2_{NXS} may also be used to estimate the M_{BH} of AGNs. This led Nikolajuk et al. (2004) to propose a simple method for estimating the M_{BH} for AGNs:

$$M_{BH} = C(T - 2\Delta t)/\sigma^2_{NXS}, \quad (8)$$

where T and Δt are the light curve length and bin size of a given observation. It is a very simple and straightforward method to estimate the M_{BH} as long as the σ^2_{NXS} of the source has been estimated and the constant C is known. Given T and Δt, equation (8) indicates that the M_{BH} estimate is sensitive to the variability amplitude. The black hole mass of Cyg X-1 is known to be $M_{BH} = 10\ M_\odot$, so the constant C can be estimated. By calculating the mean σ^2_{NXS} from a number of *RXTE* observations of Cyg X-1, Nikolajuk et al. (2004) obtained $C = 0.96 \pm 0.02$. When using equation (8), several assumptions should be taken into account (Nikolajuk et al. 2004): (1) the slope of the PSD is 2 above ν_{bf}, (2) ν_{bf} scales linearly with M_{BH}, (3) the $f\mathcal{P}(f)$ amplitude is universal (Papadakis 2004), and (4) σ^2_{NXS} should be calculated from observations of length $T < 1/\nu_{bf}$. Moreover, the relativistic beaming effect of the emission from TeV blazars should be taken into account. Equation (8) is then modified as

$$M_{BH} = C(T - 2\Delta t)\delta/\sigma^2_{NXS}, \quad (9)$$

where δ is the Doppler factor. We take $\delta = 18$ for PKS 2155−304 (Ghisellini et al. 1998). As before, σ^2_{NXS} is the mean normalized excess variance averaged over a number of light curve segments.

XMM-Newton observations of PKS 2155−304 produced several uniformly sampled light curves with high signal-to-noise ratios (S/Ns). They are superior to the data obtained with previous satellites. We use the data of revolutions 174, 362, 450, 545-1, and 724 to estimate the black hole mass of PKS 2155−304. All 0.2–10 keV light curves were binned over 500 s. Since a reliable PSD break frequency is not available for PKS 2155−304 (but see Kataoka et al. 2001), for conservative purposes we broke each original light curve into several parts with each containing 20 points; thus, the length of the light curves used is $T = 10$ ks. We obtained a total of 33 such short but consecutive light curves. We calculated σ^2_{NXS} for each light curve. These σ^2_{NXS} estimates represent the variability amplitude integrated between 1 and 10 ks, almost corresponding to the gap in the PSDs derived with *ASCA*, *BeppoSAX*, and *RXTE* data (e.g., Zhang et al. 2002). The mean of the 33 σ^2_{NXS} values is 1.07×10^{-3}. Finally, we used this mean σ^2_{NXS} to derive the black hole mass by using equation (9). The derived black hole mass is $\sim1.45\times10^8\ M_\odot$. Without correction for the relativistic beaming effect, the derived black hole mass would be $\sim8.05\times10^6\ M_\odot$, consistent with the value of M_{BH} derived with the normalized PSD by Hayashida et al. (1998) and Czerny et al. (2001).

5. DISCUSSION

Variance estimates provide a simple but useful way of quantifying the variability of blazars. However, the stochastic nature of the red-noise process means that only the average properties of the variance can provide physical insight. Due to inadequate coverage, previous estimates of the variance in TeV blazars were based only on individual light curves. Because of the large scatter in the variance intrinsic to the red-noise variability, the changes in individual variances usually provide less insight than expected. The important issue is how to disentangle the changes in the variance produced by the scatter in the variance of a stationary process from real changes in the variance due to the underlying physical process responsible for the variability. In order to determine the variability of TeV blazars that exhibit the most significant X-ray variability among blazars, we have applied several methods relevant to the variance estimate to a number of high-quality X-ray light curves of PKS 2155−304 obtained with *XMM-Newton*.

We first calculated the individual variance estimates using 500 s long segments of the light curves binned on timescales of 25 s and compared them with the expected scatter around the mean using the Monte Carlo simulation results of stationary processes (Vaughan et al. 2003b). Our results showed that the observed individual variances of PKS 2155−304 were well within the confidence range expected for a stationary process.

This is consistent with the idea that the underlying physical process responsible for the source variability is stationary. However, it is worth noting that the expected scatter in variance is rather large for the red-noise data (more than 1 order of magnitude for a PSD with a slope of 2 adopted for PKS 2155−304). The real changes in the variability amplitude may be much smaller than this scatter. If this is the case, the real changes in the variability amplitude cannot be revealed by this method.

As averaging over many independent variance estimates reduces the random scatter inherent in the red-noise data, real changes in the variability amplitude can be measured from the mean variances. There are two ways to average the variances. First, the averaged variance and its error can be calculated by binning the individual consecutive variance estimates; this gives rise to the evolution of the averaged variance with time. Whether the averaged variance changes with time or not can be tested through fitting the mean variances with a constant. Our results indicate that the averaged variance changes with time during flare states, suggesting nonstationary variability. In the second way, the individual variance estimates were sorted and binned according to the count rates. In this way, the relationship between averaged variances and fluxes can be constructed. Interestingly, we obtained two kinds of correlations in opposite senses: the mean absolute rms variability amplitude linearly correlates with flux, but $F_{\rm var}$ linearly anticorrelates with flux. Although the first correlation may be artificial due to a linear correlation between variance and flux, the correlation between $F_{\rm var}$ and flux should reflect real changes of the averaged variance with flux. Since a random scatter in the variance of the red-noise variability should not give rise to any correlation between $F_{\rm var}$ and flux, the anticorrelation between $F_{\rm var}$ and flux shows that the underlying physical process responsible for the variability of PKS 2155−304 is not stationary. This genuine nonstationarity of the underlying process reflects real changes in the physical conditions of the variability process, such as the physical parameters of the emitting region.

The mean properties of a stochastic process have frequently been applied in the timing studies of X-ray binaries and Seyfert galaxies. The PSDs of X-ray binaries, estimated from the averaged periodogram of an ensemble light curves, evolve with time, indicating that the variability process is strongly nonstationary (e.g., van der Klis 1995). It was also found in X-ray binaries and Seyfert 1 galaxies that the mean absolute rms variability amplitude scales linearly with the flux of the source (Uttley & McHardy 2001; Vaughan et al. 2003b), indicating that the variability of these systems is intrinsically nonstationary.

More importantly, there may be two types of strong nonstationarity: (1) the strong nonstationarity due to the nonlinearity inherent in the rms–flux relation and (2) the strong nonstationarity due to a changing PSD (which would yield averaged $F_{\rm var}$ values that evolve with flux or time). In Seyfert galaxies, the rms–flux relation is one form of strong nonstationarity (since the averaged rms variability amplitude changes with time). However, this form of nonstationarity can be "factored out" by studying the $F_{\rm var}$-flux relation instead (Vaughan et al. 2003b, § 7.2). The $F_{\rm var}$-flux relation in Seyfert galaxies is flat (implying a PSD that is constant over those timescales), indicating no additional forms of strong nonstationarity. In blazars, the rms–flux relation also is a form of strong nonstationarity. However, even after removing this form of strong nonstationarity, the $F_{\rm var}$-flux relation is not flat, indicating the presence of some additional form of strong nonstationarity that is not present in Seyfert galaxies (e.g., implying a PSD whose shape and/or amplitude evolves with time or flux). This provides yet another suggestion that the X-ray variability mechanism in Seyfert galaxies and blazars may be different.

The differences between the variability amplitude of simultaneous light curves at different energy bands can be reliably examined using $F_{\rm var}$ statistics. The rms spectra presented in this work were obtained on similar timescales but for different activity phases. The results show that the shape of the rms spectrum is strongly energy-dependent during the flare phase, while during the quiet phase this dependence becomes marginal or even disappears. This indicates that the emission from the source may be comprised of two components, one strongly variable and one almost steady. The variability of the variable component is strongly energy-dependent, but the nonvariable one is not. Moreover, subtle changes in the shape of the rms spectra are also visible when comparing the individual rms spectra. These may be caused by parameter changes in the emitting region. The rms spectra of PKS 2155−304 are rather different from those of Seyfert galaxies (e.g., Vaughan & Fabian [2004] for MCG −6-30-15 and Vaughan et al. [2003b] for Mrk 766), indicating rather different emission mechanisms. The rms spectral shapes for MCG −6-30-15 also clearly changed with flux but in a different way than those for PKS 2155−304: the rms spectra of PKS 2155−304 monotonically increased with energy, while the rms spectra of MCG −6-30-15 are characterized by sporadic features (Vaughan & Fabian 2004). This may be related to the fact that blazars are jet-dominated nonthermal systems, while Seyfert galaxies are disk-dominated thermal systems. Furthermore, the point-to-point variability amplitude may track the rms spectrum, indicating that the PSD slope of PKS 2155−304 is energy-independent and in turn indicating that the PSD amplitude should be larger with increasing energy, as the rms spectrum is an increasing function of energy.

The black hole mass of some AGNs, including two blazars (3C 273 and PKS 2155−304), has been inferred with the linear scaling law of the PSD characteristics between AGNs and Cyg X-1. The PSD characteristics used includes the break frequency and a specific PSD value in $f\mathcal{P}(f)$ representation (e.g., Hayashida et al. 1998; Czerny et al. 2001; Uttley et al. 2002; Markowitz et al. 2003; Papadakis 2004). Hayashida et al. (1998) derived the $M_{\rm BH}$ for PKS 2155−304 as $\sim 8.92\times10^6\ M_\odot$. On the basis of the new PSD results for Cyg X-1, Czerny et al. (2001) found the $M_{\rm BH}$ of PKS 2155−304 as $\sim 2.45\times10^7\ M_\odot$, a factor of 2.8 larger. They determined the $M_{\rm BH}$ of PKS 2155−304 by assuming that the temporal frequency (or timescale) at $f\mathcal{P}(f) = 10^{-3}$ is linearly scaled with the $M_{\rm BH}$ and taking $M_{\rm BH} = 10\ M_\odot$ for Cyg X-1 as the reference point. However, calculating the PSD is very complicated; in particular, very few PSDs are available for blazars. The method proposed by Nikolajuk et al. (2004) provides a simple way to infer $M_{\rm BH}$ in AGNs, which requires the estimates of $\sigma^2_{\rm NXS}$ only and should be applicable to many more cases than the methods based on the PSD. The assumptions of both methods are the same. Using this method, we obtained the $M_{\rm BH}$ of PKS 2155−304 as $\sim 8.05\times10^6\ M_\odot$, consistent with the value obtained by Hayashida et al. (1998). After correcting for the relativistic beaming effect, the black hole mass of PKS 2155−304 is $\sim 1.45\times10^8\ M_\odot$ (assuming the Doppler factor $\delta = 18$). Using *RXTE* and *ASCA* data, the $M_{\rm BH}$ values of Seyfert galaxies estimated with $\sigma^2_{\rm NXS}$ are in agreement with those obtained with other methods (Nikolajuk et al. 2004).

XMM-Newton provides a large number of blazar light curves with a typical exposure time of ∼40 ks. Because of its high output and long orbital period, the *XMM-Newton* light curves are evenly sampled and have high S/N. *XMM-Newton* therefore

provides us with a good opportunity to estimate the $M_{\rm BH}$ of blazars from $\sigma^2_{\rm NXS}$, which can be compared with the $M_{\rm BH}$ obtained from other methods, such as the stellar velocity dispersion from the optical spectra of the host galaxies of blazars (e.g., Barth et al. 2003; Falomo et al. 2003a). Since no values of the velocity dispersion of the galaxy PKS 2155−304 are available so far, its black hole mass has not yet been inferred with this (velocity dispersion) method. However, we note that for the dozen BL Lac objects for which the velocity dispersion of the galaxy has been directly measured, one finds black hole masses on the order of $10^9\,M_\odot$ for BL Lac objects (Falomo et al. 2003b). Moreover, the observed host galaxy luminosity ($R = -24.4$, $H = -26.8$) also yields black hole masses on the order of $10^9\,M_\odot$ for BL Lac objects (Kotilainen et al. 1998; Falomo et al. 2003b). The black hole mass of PKS 2155−304 derived using X-ray variability is smaller by 1 order of magnitude than these, but the uncertainty is substantial. This possible inconsistency is worth studying with more X-ray data for more blazars, especially for blazars for which the black hole masses have been estimated using the velocity dispersion of the host galaxy.

Finally, we mention caveats associated with using the normalized excess variance–black hole mass relation proposed by Nikolajuk et al. (2004). (1) To do a direct comparison of variability amplitudes (or PSD shapes) between different classes of objects (e.g., blazars vs. Seyfert galaxies or BHXRBs) would ideally require that the nature of the X-ray variability be the same in both classes of objects, but the link between the variability of jet-dominated X-ray emission and the variability of accretion disk corona–dominated X-ray emission is not clear. The fact that blazars may have steeper red-noise PSDs than Seyfert galaxies could be viewed as an obstacle to "unifying" their X-ray variability properties. Another such obstacle is the fact that $F_{\rm var}$ tends to increase as energy increases in (jet dominated) blazars, while the opposite is generally true for (disk dominated) radio-quiet Seyfert galaxies (e.g., above 2 keV; see Vaughan et al. [2003b] for Mrk 766 and Vaughan & Fabian [2004] for MCG −6-30-15). (2) The observation that $F_{\rm var}$ decreases as flux increases in PKS 2155−304 could imply that the time-averaged PSD shape and/or amplitude changes as source luminosity increases. Physically, since the black hole mass of the source cannot evolve rapidly over the course of a few hours, this could mean that $F_{\rm var}$ and the PSD of PKS 2155−304 may depend more on some other physical properties and less directly on black hole mass. In contrast, all Seyfert galaxies have a universal PSD shape that shifts toward lower temporal frequencies as one considers higher source black hole mass (and the variability is "slower" for higher mass objects). However, PSDs for individual Seyfert galaxies do not seem to evolve on timescales shorter than years (e.g., Markowitz & Edelson 2001, 2004). (3) The different $F_{\rm var}$-flux relations indicate that the X-ray variability mechanism in Seyfert galaxies and blazars may be different.

6. CONCLUSIONS

Using simple variance statistics, we have studied the X-ray variability properties of the TeV blazar PKS 2155−304 with several high-S/N, consecutive light curves obtained with the *XMM-Newton* EPIC pn camera during a period of about 3 yr. The main conclusions are as follows (even though comparison to other blazars should ideally take precedence):

1. The individual excess variance (or normalized variance) estimates, calculated with 500 s long segments of the 25 s binned light curves, are within the expected scatter around the mean for a red-noise process, consistent with the assumption that the X-ray variability of PKS 2155−304 is the result of a stationary process.
2. The mean excess variance and fractional rms variability amplitude, calculated by binning consecutive individual estimates in time, change with time during flare states, indicating that the processes responsible for the X-ray variability of PKS 2155−304 are strongly nonstationary.
3. However, the mean absolute and fractional rms variability amplitude, calculated by sorting and binning the individual estimates according to count rates, show an opposite correlation with flux. The absolute rms variability amplitude linearly correlates with flux, but the fractional rms variability amplitude linearly anticorrelates with flux. These two kind of correlations suggest that there may be two types of strong nonstationarity in the X-ray variability of PKS 2155−304. The latter correlation supports a strong nonstationary origin of the X-ray variability.
4. During significant variations, $F_{\rm var}$ shows a strong dependence on energy: the fractional rms variability amplitude increases logarithmically with increasing energy. The ratio of $F_{\rm var}$ to $F_{\rm pp}$ is possibly energy-independent, suggesting that the PSD slope of the source is energy-independent, while the PSD amplitude should be larger for higher energy.
5. Using the normalized excess variance, we estimated the black hole mass of PKS 2155−304 as $\sim 1.45\times10^8\,M_\odot$.

We are grateful to the anonymous referee for the constructive suggestions and comments that greatly improved the manuscript. This work is based on observations obtained with *XMM-Newton*, an ESA science mission with instruments and contributions directly funded by the ESA Member States and the USA (NASA). This work is conducted under Project 10473006, supported by the National Natural Science Foundation of China, and under a project sponsored by the Scientific Research Foundation for the Returned Overseas Chinese Scholars, State Education Ministry. This work is also financially supported in part by the Directional Research Project of the Chinese Academy of Science under project KJCX2-SW-T08.

REFERENCES

Barth, A. J., Ho, L. C., & Sargent, W. L. W. 2003, ApJ, 583, 134
Belloni, T., & Hasinger, G. 1990, A&A, 227, L33
Belloni, T., Psaltis, D., & van der Klis, M. 2002, ApJ, 572, 392
Bevington, P. R., & Robinson, D. K. 1992, Data Reduction and Error Analysis for the Physical Sciences (New York: McGraw-Hill)
Bian, W. H., & Zhao, Y. H. 2003, MNRAS, 343, 164
Blandford, R., & Rees, M. 1978, Phys. Scr., 17, 265
Brinkmann, W., Papadakis, I. E., den Herder, J. W. A., & Haberl, F. 2003, A&A, 402, 929
Cui, W. 2004, ApJ, 605, 662
Czerny, B., Nikołajuk, M., Piasecki, M., & Kuraszkiewicz, J. 2001, MNRAS, 325, 865
Edelson, R., Turner, T. J., Pounds, K., Vaughan, S., Markowitz, A., Marshall, H., Dobbie, P., & Warwick, R. 2002, ApJ, 568, 610
Edelson, R. A., Griffiths, G., Markowitz, A., Sembay, S., Turner, M. J. L., & Warwick, R. 2001, ApJ, 554, 274
Edelson, R. A., Pike, G. F., & Krolik, J. H. 1990, ApJ, 359, 86
Falomo, R., Carangelo, N., & Treves, A. 2003a, MNRAS, 343, 505
Falomo, R., Kotilainen, J. K., Carangelo, N., & Treves, A. 2003b, ApJ, 595, 624
Fossati, G., et al. 2000, ApJ, 541, 153
Ghisellini, G., Celotti, A., Fossati, G., & Comastri, A. 1998, MNRAS, 301, 451
Hayashida, K., Miyamoto, S., Kitamoto, S., Negoro, H., & Inoue, H. 1998, ApJ, 500, 642

Kataoka, J., et al. 2001, ApJ, 560, 659
Kotilainen, J. K., Falomo, R., & Scarpa, R. 1998, A&A, 336, 479
Leighly, K. 1999, ApJS, 125, 297
Maraschi, L., et al. 2005, in New Visions of the X-Ray Universe in the *XMM-Newton* and *Chandra* Era, ed. F. Jansen (ESA SP-488; Noordwijk: ESA), in press (astro-ph/0202418)
Markowitz, A., & Edelson, R. 2001, ApJ, 547, 684
———. 2004, ApJ, 617, 939
Markowitz, A., et al. 2003, ApJ, 593, 96
Massaro, E., Perri, M., Giommi, P., & Nesci, R. 2004, A&A, 413, 489
McHardy, I. M., Papadakis, I. E., Uttley, P., Page, M. J., & Mason, K. O. 2004, MNRAS, 348, 783
Nandra, K., George, I. M., Mushotzky, R. F., Turner, T. J., & Yaqoob, T. 1997, ApJ, 476, 70
Nikolajuk, M., Papadakis, I. E., & Czerny, B. 2004, MNRAS, 350, L26
Paltani, S. 1999, in ASP Conf. Ser. 159, BL Lac Phenomenon, ed. L. O. Takalo (San Francisco: ASP), 293
Papadakis, I. E. 2004, MNRAS, 348, 207
Pian, E. 2002, PASA, 19, 49
Pottschmidt, K., et al. 2003, A&A, 407, 1039
Press, W. H. 1978, Comments Astrophys., 7, 103
Press, W. H., & Rybicki, G. B. 1997, in Astronomical Time Series, ed. D. Maoz, A. Sternberg, & E. M. Leibowitz (Dordrecht: Kluwer), 61
Press, W. H., Teukolsky, S. A., Vetterling, W. T., & Flannery, B. P. 1992, Numerical Recipes (Cambridge: Cambridge Univ. Press)
Ravasio, M., Tagliaferri, G., Ghisellini, G., & Tavecchio, F. 2004, A&A, 424, 841
Rodríguez-Pascual, P. M., et al. 1997, ApJS, 110, 9
Sembay, S., Edelson, R., Markowitz, A., Griffiths, R. G., & Turner, M. J. L. 2002, ApJ, 574, 634
Tanihata, C., Urry, C. M., Takahashi, T., Kataoka, J., Wagner, S. J., Madejski, G. M., Tashiro, M., & Kouda, M. 2001, ApJ, 563, 569
Turner, T. J., George, I. M., Nandra, K., & Turcan, D. 1999, ApJ, 524, 667
Ulrich, M.-H., Maraschi, L., & Urry, C. M. 1997, ARA&A, 35, 445
Urry, C. M., & Padovani, P. 1995, PASP, 107, 803
Uttley, P., & McHardy, I. M. 2001, MNRAS, 323, L26
Uttley, P., McHardy, I. M., & Papadakis, I. E. 2002, MNRAS, 332, 231
Uttley, P., McHardy, I. M., & Vaughan, S. 2005, MNRAS, 359, 345
van der Klis, M. 1989, in Timing Neutron Stars, ed. H. Ogelman & E. P. J. van den Heuvel (NATO ASI Ser. C, 262; Dordrecht: Kluwer), 27
———. 1995, in X-Ray Binaries, ed. W. H. G. Lewin, J. van Paradijs, & E. P. J. van den Heuvel (Cambridge: Cambridge Univ. Press), 252
Vaughan, S., Edelson, R., Warwick, R. S., & Uttley, P. 2003a, MNRAS, 345, 1271
Vaughan, S., & Fabian, A. C. 2004, MNRAS, 348, 1415
Vaughan, S., Fabian, A. C., & Nandra, K. 2003b, MNRAS, 339, 1237
Zhang, Y. H. 2002, MNRAS, 337, 609
Zhang, Y. H., Cagnoni, I., Treves, A., Celotti, A., & Maraschi, L. 2004, ApJ, 605, 98
Zhang, Y. H., et al. 1999, ApJ, 527, 719
———. 2002, ApJ, 572, 762